Cell J
Cell Journal(Yakhteh) Homepage: https://www.celljournal.org/
Original Article Vol 25, No 1, January 2023, Pages: 35-44

Effects of Different Perfusing Routes through The Portal Vein, Hepatic Vein, and Biliary Duct on Whole Rat Liver Decellularization

Bahram Jambar Nooshin, M.Sc.[1], Tahereh Tayebi, Ph.D.[1], Amirhesam Babajani, M.D.[2], Mohammad-Mehdi Khani, Ph.D.[1*], Hassan Niknejad, Ph.D.[2*]

1. Department of Tissue Engineering and Applied Cell Sciences, School of Advanced Technologies in Medicine, Shahid Beheshti University of Medical Sciences, Tehran, Iran
2. Department of Pharmacology, School of Medicine, Shahid Beheshti University of Medical Sciences, Tehran, Iran

**Corresponding Addresses: P.O.Box: 1985717446, Department of Tissue Engineering and Applied Cell Sciences, School of Advanced Technologies in Medicine, Shahid Beheshti University of Medical Sciences, Tehran, Iran*
P.O.Box: 1985717446, Department of Pharmacology, School of Medicine, Shahid Beheshti University of Medical Sciences, Tehran, Iran
Emails: khani@sbmu.ac.ir, niknejad@sbmu.ac.ir

Received: 11/July/2022, Revised: 11/September/2022, Accepted: 04/October/2022

Abstract

Objective: Organ transplantation is the last therapeutic choice for end-stage liver failure, which is limited by the lack of sufficient donors. Decellularized liver can be used as a suitable matrix for liver tissue engineering with clinical application potential. Optimizing the decellularization procedure would obtain a biological matrix with completely removed cellular components and preserved 3-dimensional structure. This study aimed to evaluate the decellularization efficacy through three anatomical routes.

Materials and Methods: In this experimental study, rat liver decellularization was performed through biliary duct (BD), portal vein (PV), and hepatic vein (HV); using chemical detergents and enzymes. The decellularization efficacy was evaluated by measurement of DNA content, extracellular matrix (ECM) total proteins, and glycosaminoglycans (GAGs). ECM preservation was examined by histological and immunohistochemical (IHC) staining and scanning electron microscopy (SEM). Scaffold biocompatibility was tested by the MTT assay for HepG2 and HUVEC cell lines.

Results: Decellularization through HV and PV resulted in a transparent scaffold by complete cell removal, while the BD route produced an opaque scaffold with incomplete decellularization. H&E staining confirmed these results. Maximum DNA loss was obtained using 1% and 0.5% sodium dodecyl sulfate (SDS) in the PV and HV groups and the DNA content decreased faster in the HV group. At the final stages, the proteins excreted in the HV and PV groups were significantly less than the BD group. The GAGs level was diminished after decellularization, especially in the PV and HV groups. In the HV and PV groups the collagen amount was significantly more than the BD group. The IHC and SEM images showed that the ECM structure was preserved and cellular components were entirely removed. MTT assay showed the biocompatibility of the decellularized scaffold.

Conclusion: The results revealed that the HV is a more suitable route for liver decellularization than the PV and BD.

Keywords: Biliary Duct, Decellularization, Hepatic Vein, Portal Vein, Tissue Engineering

Citation: **Jambar Nooshin B, Tayebi T, Babajani A, Khani MM, Niknejad H. Effects of different perfusing routes through the portal vein, hepatic vein, and biliary duct on whole rat liver decellularization. Cell J. 2023; 25(1): 35-44. doi: 10.22074/CELLJ.2022.557600.1081.**
This open-access article has been published under the terms of the Creative Commons Attribution Non-Commercial 3.0 (CC BY-NC 3.0).

Introduction

Chronic and acute liver diseases are growing challenges responsible for approximately 2% of total deaths worldwide (1). Liver transplantation is the last treatment option in end-stage liver disease; however, shortage of transplantable tissues is the major obstacle for this therapeutic approach (2). In order to surmount this challenge, engineering liver tissue by employing decellularization-recellularization techniques has become a valuable strategy in recent years (3). The decellularization technique aims to provide a healthy cell-free tissue with preserved extracellular matrix (ECM) composition, intact 3D macro- and micro-structure, and a maintained vascular network. Subsequently, the decellularized scaffold could be engineered by recellularization. These cells then attach onto the scaffold, proliferate, differentiate, become functional, and create a new engineered tissue for tissue transplantation (4).

ECM consists of functional and structural molecules, which play a pivotal role in the viability, proliferation, and differentiation of transferred cells after re-cellularization (5). Thus, preserving the bio-architecture of the ECM with the maximum bioactive molecules is a pivotal aspect of tissue engineering. Different decellularization strategies have been designed utilizing single or multi-step mechanical, chemical, and enzymatic protocols, leading to various undesirable structural and compositional effects on decellularized ECM (6). Optimizing decellularization methods has become an interesting issue for researchers in order to reduce the destructive impact of the current techniques by selecting suitable material and conditions regarding cellular density, specific ECM structure, physiological function, and anatomy of aimed tissue (7). The optimized decellularization method is a rapid and effective procedure for cell destruction and removal of the cell membrane, cytoplasmic organelles, and nuclear

content debris from the tissue in the shortest time. Simultaneously, maintaining the structural components of tissue scaffold such as various collagen types, laminin, fibronectin, and glycosaminoglycans (GAGs) and preventing washing of growth factors, cytokines, and other signaling molecules out of the ECM are essential parameters in an optimized decellularization protocol (8). The controversial challenge of decellularization protocols is balancing between cellular debris removal that reduces the immunogenicity problems of the ECM and preserving the crucial components of the scaffold that is pivotal for cellular function after re-cellularization (9, 10). Therefore, designing a non-immunogenic, non-toxic, and non-pathogenic scaffold depends on utilizing effective decellularization strategies. The primary cause of decellularized scaffold immunogenicity is the remaining cellular DNA, RNA, and membrane antigenic epitopes, as well as decellularizing agents such as detergents in the ECM (11). Thus, removing antigens from decellularized scaffold as much as possible will reduce the chance of immune reaction.

In order to increase the decellularization efficacy and reduce immunogenicity, selecting an appropriate access route for infusing decellularization agents is pivotal. The common way to whole organ decellularization is the use of the main blood supply vein and artery of the organ to achieve the optimum decellularized scaffold, but the blood circulation system of the liver is quite specific and unique to this organ. Unlike other organs, the liver possesses four major routes including three main blood vessels [the portal vein (PV) and hepatic artery (HA) as blood entry routes, and the hepatic vein (HV) as the only blood outlet], and bile duct (BD) network which originates from the depths of the liver tissue. The vascular network in the structural units of the liver (sinusoids) contains three branches of vessels and a biliary duct (BD) as part of the biliary system (12). The rapid penetration rate of decellularization agents in each part of the liver, which is critical for decellularization efficacy, depends on the administration route. The present study aims to demonstrate the success rate of whole rat liver decellularization by administration of decellularizing agents through different routes, including PV, HV and BD in similar conditions.

Material and Methods

Rat liver isolation

In this experimental study, adult male Sprague-Dawley rats (200-300 g) were used to provide the intact liver. The animals were kept under standard controlled environment conditions (12:12 hours. light/dark cycle) with free access to food and water. The rats were anesthetized by intraperitoneal injection (IP, 0.1 ml/kg) of ketamine/xylazine cocktail based on the guideline of the Institutional Animal Care and Use Committees (IACUC). After skin disinfection, animals were placed in an abdominal surgery position, and a U-shaped incision was performed to expose the abdominopelvic cavity. BD (26 G), PV (24 G), and HV (22 G) were cannulated by an intravenous catheter (Tabanmedic, IR). Besides, the hepatic artery and superior vena cava were ligated by a 4-0 silk suture. Subsequently, 0.5 ml of 200 IU/ml aqueous heparin (Daru Pakhsh, IR) solution was injected into the PV to prevent blood coagulation. Finally, the liver was removed from the abdominopelvic cavity and rinsed by 50 ml of sterile heparinized phosphate-buffered saline (PBS, 10 IU/ml) by a 0.5 ml/minute perfused flow rate and stored in PBS at 2-8˚C for starting the decellularization process.

Rat liver decellularization

According to previous studies, a chemical method consisting of a combination of detergent and enzymes was used for whole organ decellularization (13). The harvested liver was transferred to the main chamber of a home-designed decellularization bioreactor under the biological class B safety cabinet (Fig.1A). The bioreactor consists of four major parts: i. The main chamber: It is a chamber in which the liver is placed for decellularization. It has three inlet and outlet channels to connect to the routes of the liver. During the perfusion of decellularization solutions, one of the routes was selected for entry of the fluid and was connected to the perfusion inlet fluid valve and two other routes were used as fluid outlets. ii. Perfusion pumps: peristaltic pumps are designed to supply the required flow rate for decellularization solutions in the path of the inlet and outlet routes from 0.5 to 1.5 mL/minute in different steps. iii. Media reservation bottles: the chambers or bottles are installed for storage and perfusion of the solutions to the inlet route i and collection of the outlets' effluents. iv. Tubes, connectors and valves: different types and sizes of tubes, connectors and valves are designed to guide solutions into the liver at specific times and collect the effluents. Rat liver decellularization was done through one of the three different perfusion routes: BD, PV, and (HV) (Fig.1B); using a method consists of chemical detergents and enzymes.

The decellularization process was initiated by infusing Krebs-Henseleit buffer (PH=7.4) consisting of NaCl 118 mM (Merck, Germany), $NaHCO_3$ 25 mM (Merck, Germany), KCl 4.7 mM (Merck, Germany), KH_2PO_4 1.2 mM (Merck, Germany), $MgSO_4$ 1.2 mM (Merck, Germany), $CaCl_2$ 1.25 mM (Merck, Germany) and Glucose 11 mM (Merck, Germany) perfused at a 0.5 mL/minute flow rate for removing the remaining blood in the liver (14). Decellularization was continued by administrating different aqueous materials including Sodium dodecyl sulfate (SDS, Merck, Germany), Triton X100 (Merck, Germany), and sodium deoxycholate (SDC, Sigma-Aldrich, USA) with different concentrations, durations, and flow rates which are shown in Figure 1C.

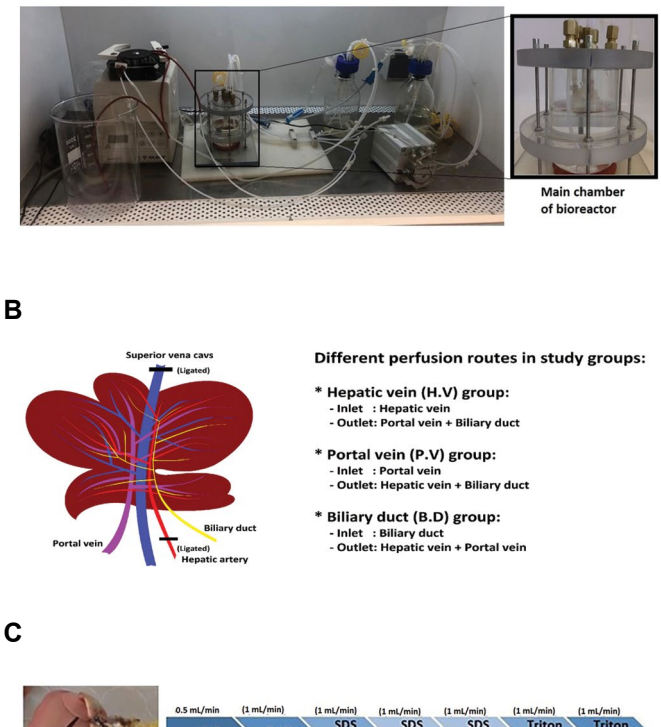

Fig.1: The bioreactor, perfusing routes and process of liver decellularization. **A.** Custom-designed whole rat liver decellularization bioreactor and its main chamber. The cannulated routes (HV, PV, and BD) of rat liver were connected to the main chamber valves letting the decellularization solutions to circulate in the liver by peristaltic perfusion pump. **B.** Schematic anatomical structure of the rat liver vascular network. **C.** Diagram of rat liver decellularization protocol illustrated by detailed information of each step, including ingredient, flow rate, and duration. The rat liver before and after the decellularization process is shown in the start and endpoint of the diagram. HV; Hepatic vein, PV; Portal vein, and BD; Biliary duct.

DNA content measurement

Measurement of total remaining DNA in the decellularized tissues was conducted for freeze-dried decellularized livers as well as the decellularization effluent during perfusion in all study groups, using the DNeasy Blood & Tissue Kit (QIAGEN, Germany). Briefly, total DNA was extracted from 1mL of effluent samples and 15mg of dried tissue according to the kit's instructions. DNA concentration was measured using a Nanodrop spectrophotometer (ND2000, Thermo, USA) at 260 nm. The data of DNA content was normalized to 1mL of effluent volume or 1mg of dried tissue weight. Equal volumes of the extracted DNA of the decellularized scaffold were loaded onto 1% (w/v) agarose gel and electrophoresed with a 100 bp DNA ladder (Invitrogen-15628019, USA) to investigate DNA fragments.

Histological evaluation of extracellular matrix structure

Freshly isolated and decellularized liver scaffolds were fixed by 10% formalin solution for 24-48 hours. After dehydration by a series of ascending ethanol concentrations (60-100% v/v) and immersion in Xylene (Merck, Germany), tissues were embedded in paraffin. The samples were cut into 5 µm thickness slides with a microtome (MICRO DS, 4055) and stained with standard Hematoxylin-Eosin (H&E). The sample slides were also stained with 300nM DAPI (4', 6-diamidino-2-phenylindole di-hydrochloride, Sigma-Aldrich, USA) solution to assess the removal of the nuclear components of the scaffold. The sections of decellularized liver samples were also stained by Masson Trichrome and Van Gieson for investigation of the ECM network structure.

Total protein measuring assay

To evaluate the total protein content of the decellularization effluents, we measured the total protein concentration by the Pyrogallol red assay kit (BIOREX diagnostic, UK) based on a colorimetric assay with optical absorbance at 600 nm. After each decellularization step, the effluent was sampled and the total protein content was evaluated after papain digestion, hydrolyzation, and neutralization as were described in the previous section. The total protein amount was normalized to 1 mL of effluent volume.

Extracellular matrix component measuring assay

For a detailed evaluation of ECM composition, the amounts of remaining collagen and GAGs in the decellularized tissue were measured. Intact and decellularized liver tissues were cut into small pieces and lyophilized. Subsequently, samples were weighed and digested with Papain (Sigma-Aldrich, USA, 150 µg/mL) at 60˚C overnight. The contents of the GAGs were evaluated according to Farndale et al. (15) with the colorimetric reaction between DMMB (1,6-dimethylmethylene blue, Sigma-Aldrich, US) and GAGs at 525 nm. Afterward, the collagen contents were quantified indirectly using a colorimetric assay to detect hydroxyproline, as described by Reddy and Enwemeka (16). Briefly, papain digested samples were hydrolyzed with 6 N HCL at 105˚C for 18 hours. The hydrolyzed samples were neutralized by 5 N NaOH and then oxidized with Chloramine-T (Merck, Germany). Finally, the samples were reacted with para-dimethylaminobenzaldehyde (Thermo Fisher, USA). The optical absorbance at 570 nm indicated the amount of hydroxyproline in the samples. Collagen values were calculated assuming 12.5% of collagen is hydroxyproline. The amounts of collagen and GAGs were normalized to 1mg of dried tissue weight.

Scanning electron microscopy

For ultrastructural investigation of the decellularized scaffold of rat liver, samples were fixed in a 2%

glutaraldehyde solution for 24-48 hours at room temperature. The samples were washed three times with fresh PBS. After the dehydration process by a series of ascending ethanol solutions (60-100% v/v), the samples were prepared for scanning electron microscopy (SEM) by a chromium-coated sputter. The ultrastructure of the ECM was visualized using a JEOL 7401F field emission electron microscope.

Immunohistochemical analysis

We performed immunohistochemistry (IHC) staining to determine the critical protein content of the decellularized liver scaffold. After processing the samples using the standard tissue protocol, same as for H&E staining, the samples were permeabilized, and antigen retrieval was done. The primary antibodies including rabbit anti-rat collagen type I (1:500, Millipore-AB755P, Germany), rabbit anti-rat collagen type II (1:250, Millipore-AB2036, Germany), goat anti-rat collagen type IV (1:100, Millipore-AB769, Germany), rabbit anti-rat laminin (1:200, Abcam-AB11575, USA) and rabbit anti-rat fibronectin (1:250, Abcam-AB2413, USA) were used in IHC staining.

Evaluation of cell proliferation on decellularized scaffolds

Cell proliferation on decellularized liver scaffolds was examined using the MTT assay. Both HepG2 (as a hepatocyte model) and HUVEC (as an endothelial cell model) cell lines were used separately in this investigation. The HV, PV, and BD decellularized liver scaffolds were cut into cubic form (5×5×5 mm) and kept overnight in 24-well plates in DMEM. Afterwards, the medium was renewed by DMEM medium containing 10% FBS, 1% penicillin/streptomycin, 100 mM sodium pyruvate, and 1.5 g/L sodium bicarbonate. The cells were suspended at a density of 2×10^6 cells per 50 µL (for each cubic decellularized scaffold), filled in a 0.5 mL insulin syringe, and released drop by drop onto the scaffolds. To allow cell attachment, the seeded scaffolds were placed in an incubator for 1 hour and followed by the addition of cell culture medium with a total volume of 1.2 mL per well on day 0. The same density of cells cultured in the culture plate was used as control. The MTT assay was performed at 1, 2, 3, and 7 days after cell culture by replacing the medium and adding 0.5 mg/ml MTT solution to each well and incubating at 37˚C for four hours. In the final step, all medium was slowly removed and 500 µL dimethyl sulfoxide (DMSO) was added to dissolve the formazan crystals. The absorbance of the well solution was measured at 570 nm using a microplate reader (Mindray plate reader MR-96A).

Statistical analyses

To achieve reproducible results, each independent decellularization group consisted of five samples, and all experiments were repeated at least three times. All statistical analyses were done using the Graph Pad Prism 8 software (GraphPad Software, USA) and were represented as mean ± standard deviation (SD). The results were compared by analyzing with one-way ANOVA and Tukey's tests to determine the significance of differences between groups were $P<0.05$ were considered statistically significant.

Ethics

This study was approved by research Ethics Committees of School Medicine, Shahid Beheshti University of Medical Sciences (IR.SBMU.MSP.REC.1398.756).

Results

Rat liver decellularization

Isolation and decellularization of rat liver were conducted using the decellularization protocol and selecting the infusion routes amongst the hepatic vein, portal vein, and biliary duct. The total decellularization time, including initial, middle and final washing steps, was less than 10 hours.

Macroscopic evaluations demonstrated that the decellularized scaffold was transparent with vascular network appearance in the PV and HV groups. No visible macroscopic difference was detected between these two groups, while the decellularized scaffold of the BD group had an opaque and unclear appearance, which showed incomplete liver decellularization (Fig.2A-C).

The H&E stained slides of intact and decellularized tissue revealed that selecting the HV and PV routes for decellularization led to removing all cellular contents. In addition, the remaining scaffolds had a fibrillary ECM structure. In contrast, in the BD group, cellular debris remained in parts of the scaffold, indicating that the decellularization process was incomplete (Fig.2D-F).

DNA content of extracellular matrix and effluents

Quantitative evaluation of the total DNA content of the decellularized liver scaffold in the three experimental groups demonstrated that total the DNA amounts in the HV, PV, and BD groups were 20.6 ± 5.4, 102.0 ± 11.1, and 602.8 ± 64.7 ng/mg of dry tissue, respectively (Fig.3A). These results exhibited that using the HV route for liver decellularization resulted in the lowest level of residual DNA content in the scaffold compared to the PV and BD routes. In the HV group the remaining DNA content was approximately 20.6 ng/mg of dry liver scaffold that was lower than 50 ng/mg dry weight as an accepted threshold level for approval of a tissue decellularization protocol. The DNA gel electrophoresis pattern is illustrated in Figure 3B. In the HV group, the fragment length of residual DNA was lower than 150 bp. However, a higher amount of DNA with a wide distribution of DNA fragments (approximately less than 200 bp) was seen in the PV group. On the other hand, higher amounts of DNA with longer lengths were observed in the BD group which is similar to the DNA electrophoretic pattern of intact liver. DAPI staining results also confirmed these results (Fig.3C-F).

Quantitative assessment of the effluents' total DNA revealed that the maximum amount of DNA removal occurred after using 1% and 0.5% SDS in the fourth step in the PV (1599 ± 137 µg/mL) and HV (2384 ± 413 µg/mL) groups. Besides, a significant difference ($P<0.001$) between the effluent DNA content of the HV and PV groups was observed in the maximal point at the 195th minute (Fig.3G). After that, the

effluents' DNA content in both groups decreased gradually until the last stage. In contrast, the total amount of DNA did not sharply peak at any decellularization step in the BD group; rather, relatively high amounts of DNA were removed from the liver during all stages continuously. A closer look at the last step DNA content of effluent in the HV and PV groups shows that the DNA content in the HV route reached zero faster than the PV route (Fig.3H).

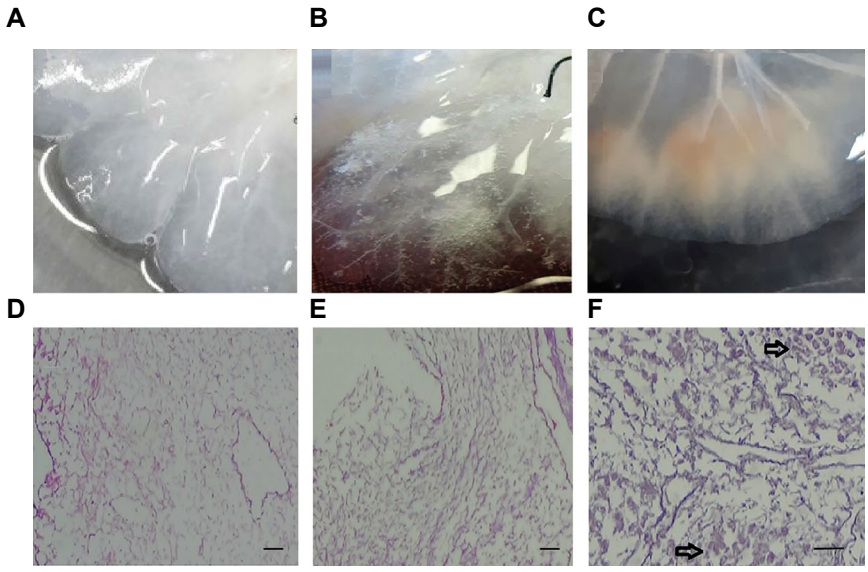

Fig.2: Macroscopic and histological evaluation of decellularizes livers. Macroscopic pictures of **A.** Decellularized liver with HV, **B.** PV and **C.** BD routes show complete decellularization in the HV and PV groups, but incomplete in the BD route group. Microscopic evaluation by H&E staining in all groups showed no cells in **D.** The HV and **E.** PV groups, but in **F.** The BD samples, some parts of the scaffold were not cleared of cells after decellularization which are shown with a black arrow in the picture (scale bar: 100 µm). HV; Hepatic vein, PV; Portal vein, and BD; Biliary duct.

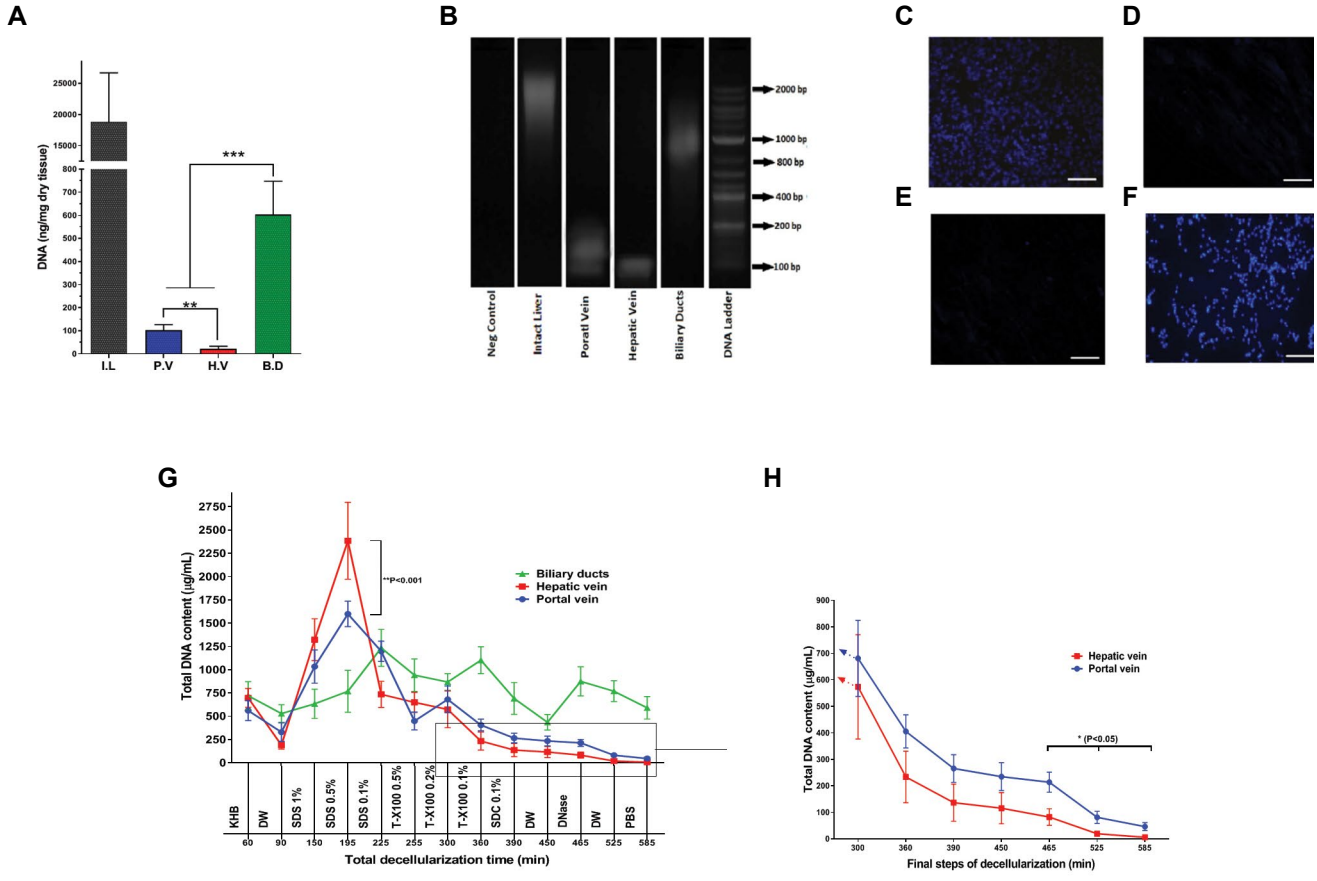

Fig.3: Evaluating the DNA content. **A.** Comparison of the DNA content of decellularized liver through the PV, HV, and BD routes with that of IL. **B.** DNA gel electrophoresis pattern in all experimental groups. **C-F.** DAPI staining in the IL, PV, HV and BD groups, respectively (scale bar: 100 µm). **G.** Effluent of the DNA content of the HV, PV, and BD groups during liver decellularization steps. **H.** Comparison of total DNA content of the decellularization effluent for the HV and PV routes at final steps. All quantitative data were analyzed through one-way ANOVA and by Tukey's tests and represented as mean ± SD (n=5). HV; Hepatic vein, PV; Portal vein, BD; Biliary duct, IL; Intact liver, *; P<0.05, **; P<0.01, and ***; P<0.001.

Total protein and extracellular matrix components of the decellularized scaffold

Data from total protein measurement demonstrated that the patterns of removing protein from the liver in all three experimental groups were relatively similar, even though there were differences among the protein concentrations and excretion times of the groups (Fig.4A). In the BD group, there was a significant delay in protein release. However, in the HV and PV groups, the protein content of the effluents were maximum after SDS solutions and subsequently decreased gradually in the next decellularization steps. The proteins excreted in the HV and PV groups were undetectable and significantly lower than the BD group in the final stages.

The results of specific methods for investigating the remaining extracellular proteins such as collagen and GAGs in decellularized scaffolds demonstrated that liver ECM proteins were affected during decellularization.

As Figure 4B shows, the total GAGs amount in the intact liver was 62.74 ± 7.28 µg/mg of dried tissue, while in the PV, HV, and BD groups, the amounts of GAGs were 25.48 ± 4.35 µg/mg, 28.36 ± 1.90 µg/mg and 43.94 ± 7.68 µg/mg, respectively. These data indicate that the total GAGs levels were diminished when cellular contents were eliminated from the liver. Although there was no difference between the PV and HV groups in GAGs levels, a significant decrease in liver GAGs amounts was seen in both mentioned groups compared with intact liver (P<0.001) and BD groups (P<0.05). Besides, the total collagen level in the intact liver (79.96 ± 7.96 µg/mg of dry tissue) was significantly lower than in the PV, HV, and BD groups (P<0.001). Total collagen levels in the decellularized scaffold by hepatic and PV routes were significantly higher (P<0.001) than the produced scaffold by the BD route (Fig.4C).

Extracellular matrix specific proteins detection

SEM images of the HV group showed that the decellularization process was successfully performed and the cells were completely removed while the ECM microstructure was preserved. (Fig.5A, B). Likewise, the images obtained from specific histological staining (Masson Trichrome and Von Geison) showed that major proteins of ECM were conserved in decellularized liver scaffolds and confirmed the absence of cells in the scaffolds (Fig.5C, D).

To better investigate the ECM protein components in the decellularized scaffold, we used IHC staining to evaluate the ECM specific proteins in the PV group as a better decellularized group according to the above results. IHC staining images revealed that the major and specific ECM proteins collagen type I, II, and IV, and laminin were preserved in the decellularized liver scaffold in the HV group (Fig.5E-H).

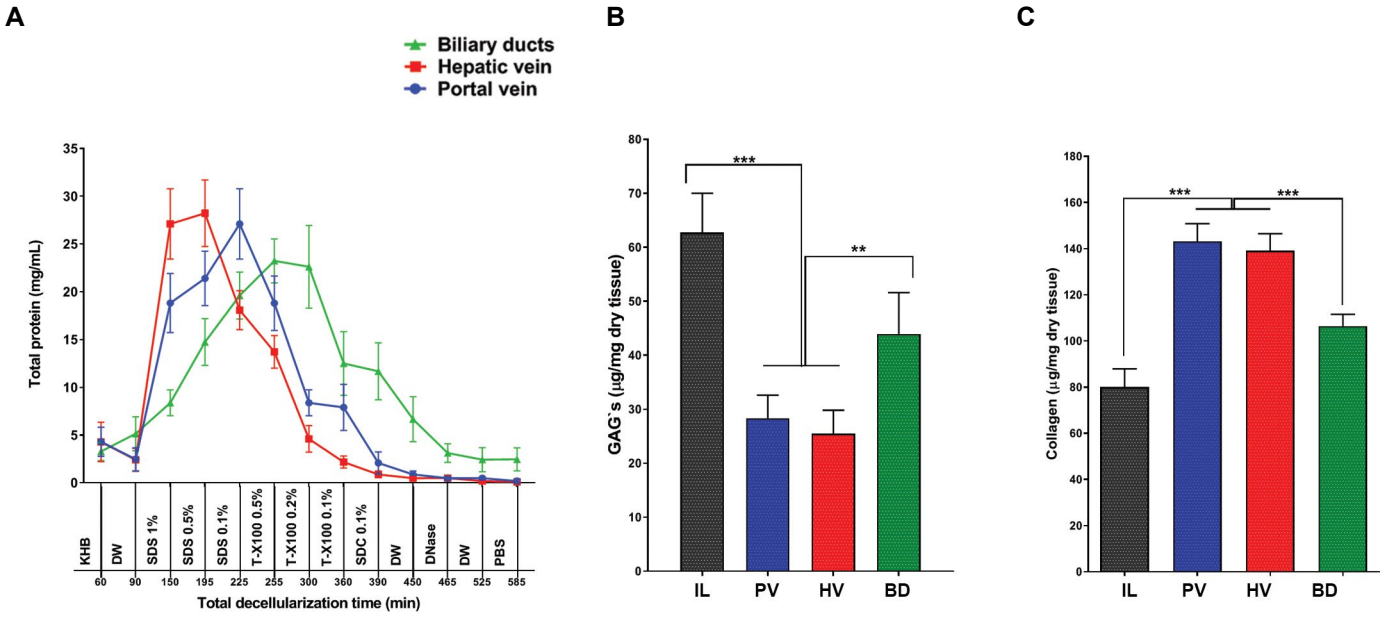

Fig.4: Quantitative comparison of ECM components. **A.** Total protein content of decellularization effluent via three different routes including the HV, PV, and BD during decellularization steps. Comparison of **B.** GAGs and **C.** Collagen contents after decellularization of rat liver via the PV, HV and BD versus IL. All data were analyzed through one-way ANOVA and by Tukey's tests and represented as mean ± SD (n=5). ECM; Extracellular matrix, HV; Hepatic vein, PV; Portal vein, BD; Biliary duct, GAGs; Glycosaminoglycans, IL; Intact liver, **; P<0.01, and ***; P<0.001.

Cytotoxicity and cell proliferation measurement

The MTT assay was used to evaluate the viability and proliferation of the cells on rat decellularized liver scaffolds at the end of days 1, 2, 3, and 7 after two cell lines culturing on the scaffolds. According to (Fig.6A), the difference between the viability of HepG2 cells in cultured plates (control) and the cells cultured on the HV, PV, and BD scaffolds was not significant during days 1 and 2. However, at days 3 and 7, the HepG2 viability for all scaffolds was significantly greater than the control group ($P<0.05$). Moreover, the viability of HepG2 cultured on scaffolds significantly increased at day 3 compared to day 2, as well as day 7 compared to day 3 ($P<0.01$ and $P<0.001$, respectively), which is an indication of cell proliferation after day 3 in the PV, HV, and BD groups.

As shown in Figure 6B, HUVEC cells viability assessment indicated a similar pattern to that of HepG2 proliferation except that in comparison with HepG2, proliferation of HUVEC cells at day 7 was more significant compared to day 3 ($P<0.0001$).

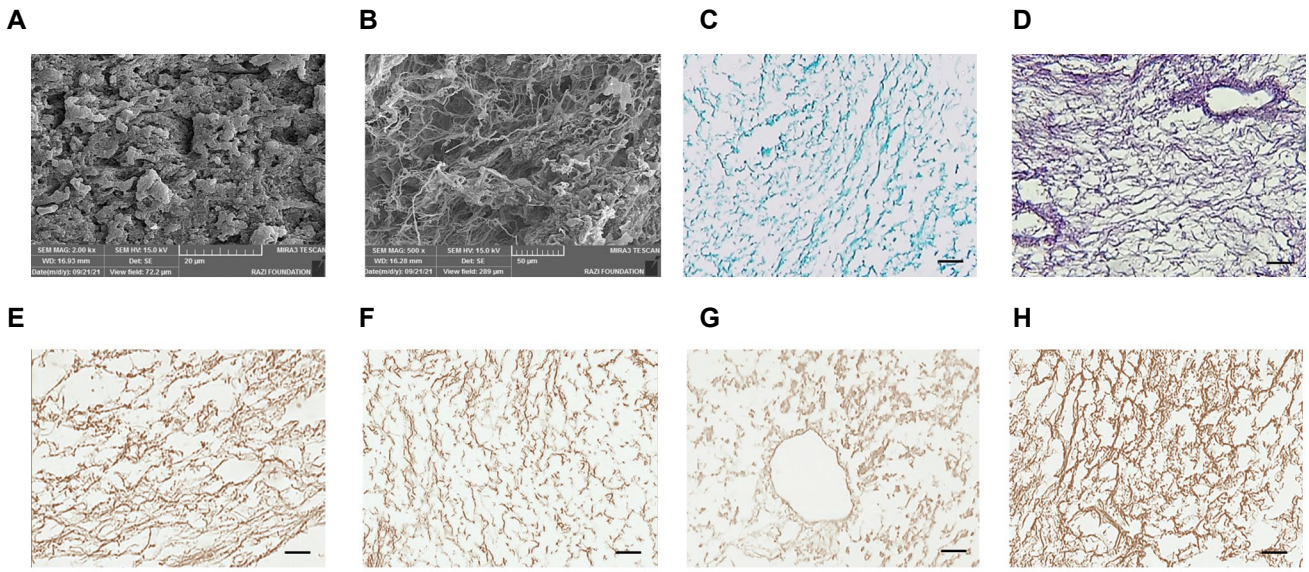

Fig.5: Evaluating the preservation of ECM component after decellularization. Representative SEM images of **A.** IL and **B.** Decellularized liver of HV group. **C.** Masson's Trichrome staining, **D.** Von Geison staining. **E.** IHC staining of collagen type I, **F.** Collagen type II, **G.** Laminin, and **H.** Collagen type IV, all for decellularized liver through the HV route (scale bar: 100 µM). ECM; Extracellular matrix, SEM; Scanning electron microscopy, IL; Intact liver, HV; Hepatic vein, and IHC; Immunohistochemical.

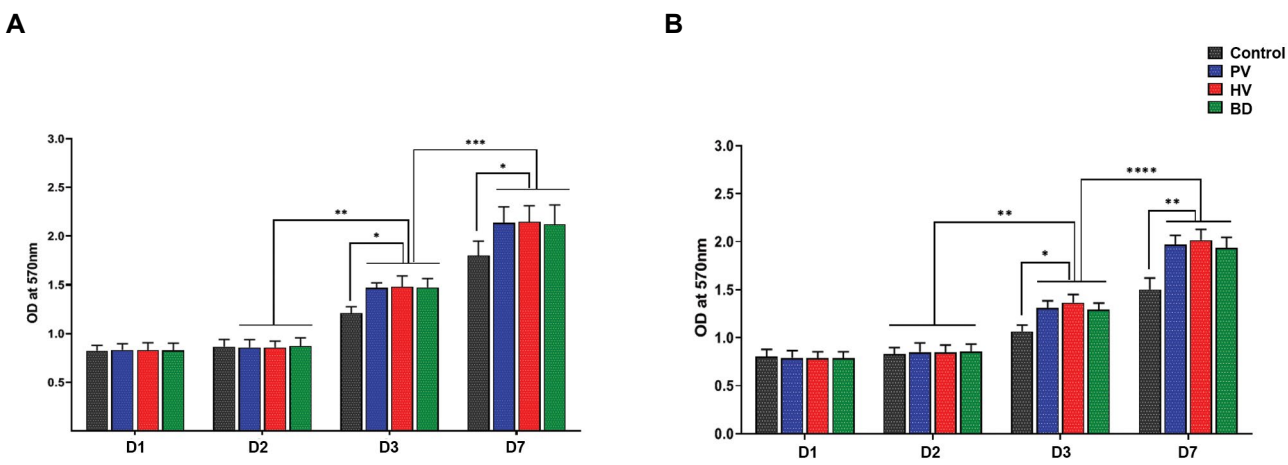

Fig.6: Cytocompatibility measurement of three types of decellularized scaffold. **A.** Evaluation of HepG2 and **B.** HUVEC viability and proliferation at days 1, 2, 3 and 7 of cell culture. All quantitative data were analyzed through one-way ANOVA and by Tukey's tests and represented as mean ± SD (n=5). HV; Hepatic vein, PV; Portal vein, BD; Biliary duct, *; $P<0.05$, **; $P<0.01$, and ***; $P<0.001$, and ****; $P<0.0001$.

Discussion

Decellularization of the whole organ has been a promising approach in tissue engineering in the recent years. This technique aims to achieve natural three-dimensional scaffolds from various allogeneic or xenogeneic origins with a preserved vascular network (17). The characteristics and quality of a decellularized scaffold are closely related to the decellularization method (18).

Many studies have evaluated different physical and chemical techniques to improve liver decellularization. For example, various detergents, different concentration of reagents, the flow rate of the solution, and perfusion conditions have been studied to improve the properties of the decellularized liver (19). But so far, there is no detailed study about the effect of the perfusion route on the outcome of the decellularization process. In this study, we evaluated the role of three different perfusion routes on rat liver decellularization.

The duration of decellularization plays an important role in the quality of the resulting scaffold. Prolonging the decellularization procedure destroys the components of the extracellular matrix, including collagen, GAGs and elastin, which leads to the weakening of the mechanical properties of the scaffold (20, 21). In this study, we reduced the decellularization time to about 8h that was enough for complete cell removal.

Tissue DNA content, visible nuclear components, and DNA fragments length are three of the most powerful tools for assessing the adequacy of tissue decellularization (22). Utilizing the PV or HV routes led to a similar pattern of DNA and protein contents in the effluents. However, this pattern was not observed in the BD route. Elution of the DNA and proteins from the liver in the PV and HV groups exhibited the effective disruption of the cellular and nuclear membrane in the first steps. Subsequently, decrease of DNA and protein contents in the middle stages indicated that most of the cells have been removed in the first stage. These results are consistent with previous decellularization studies which used the PV for liver decellularization (23, 24). In contrast, in the BD group, DNA and protein were not completely removed from the liver even during the final steps. This data revealed that decellularization through the BD was not completely successful.

One of the objects of the present study was the comparison between HV and PV routes for liver decellularization. Although there was no significant difference in the amount of the eluted proteins between these two groups, utilizing HV as the decellularization route led to a faster reduction in the amounts of DNA compared to the PV group. The DNA content in the last six decellularization steps with the HV group was significantly lower than the PV group. These results indicate that the HV is better than the PV for eluting DNA from the liver. These results demonstrate that during the decellularization process, the use of the HV route is more appropriate than the PV route in order to minimize decellularization time.

In accordance with the defined standards, the residual DNA amount should be less than 50 ng per 100 mg of the dry scaffold with no more than 200 bp length (25-27). The quantitative analysis of remaining DNA and nuclear components demonstrated that residual DNA content in the HV group was within this standard range. Furthermore, while the residual DNA length in the HV and PV groups is acceptable and DAPI staining confirmed lack of nuclear components in the decellularized scaffold in both groups, gel electrophoresis results revealed that compared to the PV group, the amount of residual DNA in the HV group is lower, DNA length is smaller, and DNA fragments length distribution is narrower. On the other hand, in the BD group we saw that higher amounts of DNA with a longer length remained, similar to the intact liver.

One of the main reasons for superiority of HV route for decellularization is the unique blood supply system of the liver, in which the PV supplies 70–75%, and the hepatic artery provides 25–30% of normal liver blood flow (28); but, total blood volume (100%) leaves the liver through the HV to maintain liver hemodynamic condition (29). Therefore, it can be concluded that the circulation capacity of the HV equals to that of the PV plus the hepatic artery. Considering the structure of liver sinusoids in which the central HV is surrounded by a triad including portal vein, hepatic artery, and biliary duct, the diameter and circulation capacity of the HV are higher than those of the PV (30). Accordingly, the time for flushing cellular debris out of the tissue was faster through the HV, so, it was better using the HV for liver decellularization.

Preservation of the ECM ultrastructure during decellularization is another critical challenge in tissue decellularization. Preservation of the structural proteins and mechanical properties of the decellularized scaffold is needed for successful production of a new engineered tissue (20). The results of IHC, specific staining of structural proteins, and electron microscopy confirmed that the ECM component and its network were preserved during decellularization through the HV or PV routes. Also, qualitative evidence of the remaining ECM proteins in the decellularized scaffold showed that in both HV and PV groups, the total GAGs and collagen levels were similar. Our data is similar to previous studies in which the total amounts of residual GAGs in the decellularized scaffolds significantly decreased in the HV and PV groups compared to the intact liver (31). It seems that this result is due to the high solubility of GAGs in aqueous solution and their removal from ECM during the decellularization protocol (31, 32). The greater collagen amount in the ECM of the HV and PV groups compared to the native and BD groups can be explained by considering the normalization method based on dry tissue weight. Intact tissues and incomplete decellularized scaffolds of the BD group mainly contain cells and insoluble collagen fibers. Thus, the weight ratio of collagen to tissue is lower than

decellularized liver. Complete decellularization mainly removes cells without insoluble collagen fibers, resulting in an increased ECM portion in dry tissue weight (9). It is necessary to consider the mentioned fact to explain controversial results from previous studies; different parameters of the decellularization protocols such as various types of detergents, concentrations, and tissues exposing time during decellularization, profoundly affect the preservation of ECM structure and content (31, 33, 34). Similar to other studies, our investigation with the IHC technique revealed that major ECM proteins, such as collagen type I, II, IV, and laminin were preserved in the HV decellularized scaffold as the best group with minimal residual DNA and maximal conserved ECM components.

Biocompatibility is the most important property of a scaffold. Studies have shown that residual decellularization agents such as SDS and Triton X100 can leave cytotoxic effects on the decellularized scaffold (35). Therefore, it is necessary to wash the tissue carefully at the end of the decellularization process. In this study, after the last step of decellularization, the decellularized tissue was thoroughly washed in two steps, with distilled water and PBS (each for one hour), respectively. Furthermore, for culture of the cells, the decellularized tissue pieces were incubated for 24 hours in DMEM to ensure the complete removal of reagents residues. Evaluating the cell viability of three types of decellularized scaffolds revealed that all scaffolds are biocompatible and suitable for cellular repopulation. These results confirmed that the decellularized liver could be used as a natural scaffold for liver regeneration (36, 37). The human liver carcinoma cell line (HepG2) is most commonly used because of the advantages of availability and maintenance, the features characteristic of normal hepatocytes (38). As well, human umbilical vein endothelial cells (HUVECs) are one of the most popular cell line used as an *in vitro* model for endothelial cells (39). We used these two different cell lines to assess cell proliferation on decellularized liver scaffolds because the liver is composed of many different cell types in which, hepatocytes and endothelial cells have some essential performances as two types of primary cells (non-parenchymal cells) (40).

More studies would be required to evaluate the recellularization efficiency of the scaffolds following different decellularization strategies. Besides, additional preclinical studies should investigate the liver function in animal models to enhance the translation of preclinical results to clinical practice.

Conclusion

The present study demonstrated that rat decellularized liver scaffold could be obtained from different decellularization routes such as the HV, PV, and BD. The results of these experiments revealed that the HV is a more suitable route than the PV for rat liver decellularization.

Acknowledgments

The authors keep alive the name and memory of the late Professor Peyravi. The authors would like to thank the staff of the Department of Pharmacology, School of Medicine, Shahid Beheshti University of Medical Sciences. Research reported in this publication is a part of a Ph.D. thesis, which was supported by Vice-Chancellor's in Research Affairs of Shahid Beheshti University of Medical Sciences, Tehran, Iran. Also, this research was supported by the Research Grant Committee from the National Institutes for Medical Research Development (NIMAD), Tehran, Iran, under award number of 963951. There is no conflict of interest in this study.

Authors' Contributions

B.J.N., H.N.; Contributed to conception and design. B.J.N.; Contributed to all experimental work, data and statistical analysis, interpretation of data, and drafted the manuscript which was revised by M.-M.K., T.T., A.B. M.-M.K.; Contributed to validation and formal analysis. T.T., A.B.; Participated in methodology and data analysis. H.N.; Was responsible for supervision. All authors read and approved the final manuscript.

References

1. Mazza G, Al-Akkad W, Rombouts K, Pinzani M. Liver tissue engineering: from implantable tissue to whole organ engineering. Hepatol Commun. 2018; 2(2): 131-141.
2. Jadlowiec CC, Taner T. Liver transplantation: current status and challenges. World J Gastroenterol. 2016; 22(18): 4438-4445.
3. Hillebrandt KH, Everwien H, Haep N, Keshi E, Pratschke J, Sauer IM. Strategies based on organ decellularization and recellularization. Transpl Int. 2019; 32(6): 571-585.
4. Zhou P, Huang Y, Guo Y, Wang L, Ling C, Guo Q, et al. Decellularization and recellularization of rat livers with hepatocytes and endothelial progenitor cells. Artif Organs. 2016; 40(3): E25-E38.
5. Wang X, Cui J, Zhang BQ, Zhang H, Bi Y, Kang Q, et al. Decellularized liver scaffolds effectively support the proliferation and differentiation of mouse fetal hepatic progenitors. J Biomed Mater Res A. 2014; 102(4): 1017-1025.
6. Keane TJ, Swinehart IT, Badylak SF. Methods of tissue decellularization used for preparation of biologic scaffolds and in vivo relevance. Methods. 2015; 84: 25-34.
7. Crapo PM, Gilbert TW, Badylak SF. An overview of tissue and whole organ decellularization processes. Biomaterials. 2011; 32(12): 3233-3243.
8. Gilpin A, Yang Y. Decellularization strategies for regenerative medicine: from processing techniques to applications. Biomed Res Int. 2017; 2017: 9831534.
9. Coronado RE, Somaraki-Cormier M, Natesan S, Christy RJ, Ong JL, Halff GA. Decellularization and solubilization of porcine liver for use as a substrate for porcine hepatocyte culture: method optimization and comparison. Cell Transplant. 2017; 26(12): 1840-1854.
10. Park KM, Park SM, Yang SR, Hong SH, Woo HM. Preparation of immunogen-reduced and biocompatible extracellular matrices from porcine liver. J Biosci Bioeng. 2013; 115(2): 207-215.
11. Hussein KH, Park KM, Kang KS, Woo HM. Biocompatibility evaluation of tissue-engineered decellularized scaffolds for biomedical application. Mater Sci Eng C Mater Biol Appl. 2016; 67: 766-778.
12. Abshagen K, Kuhla A, Genz B, Vollmar B. Anatomy and physiology of the hepatic circulation. In: Lanzer P, editor. PanVascular medicine. Berlin, Heidelberg: Springer Berlin Heidelberg; 2015: 3607-3629.
13. Gilbert TW. Strategies for tissue and organ decellularization. J Cell Biochem. 2012; 113(7): 2217-2222.
14. De Kock J, Ceelen L, De Spiegelaere W, Casteleyn C, Claes P, Vanhaecke T, et al. Simple and quick method for whole-liver decellularization: a novel in vitro three-dimensional bioengineering tool? Arch Toxicol. 2011; 85(6): 607-612.

15. Farndale RW, Buttle DJ, Barrett AJ. Improved quantitation and discrimination of sulphated glycosaminoglycans by use of dimethylmethylene blue. Biochim Biophys Acta. 1986; 883(2): 173-177.
16. Reddy GK, Enwemeka CS. A simplified method for the analysis of hydroxyproline in biological tissues. Clin Biochem. 1996; 29(3): 225-229.
17. Badylak SF, Taylor D, Uygun K. Whole-organ tissue engineering: decellularization and recellularization of three-dimensional matrix scaffolds. Annu Rev Biomed Eng. 2011; 13: 27-53.
18. Gilbert TW, Sellaro TL, Badylak SF. Decellularization of tissues and organs. Biomaterials. 2006; 27(19): 3675-3683.
19. Struecker B, Butter A, Hillebrandt K, Polenz D, Reutzel-Selke A, Tang P, et al. Improved rat liver decellularization by arterial perfusion under oscillating pressure conditions. J Tissue Eng Regen Med. 2017; 11(2): 531-541.
20. Gilpin A, Yang Y. Decellularization strategies for regenerative medicine: from processing techniques to applications. Biomed Res Int. 2017; 2017: 9831534.
21. Fazelian-Dehkordi K, Ardekani SFM, Talaei-Khozani T. Quality comparison of decellularized omentum prepared by different protocols for tissue engineering applications. Cell J. 2022; 24(5): 267-276.
22. Gilbert TW, Freund JM, Badylak SF. Quantification of DNA in biologic scaffold materials. J Surg Res. 2009; 152(1): 135-139.
23. Wang Y, Bao J, Wu Q, Zhou Y, Li Y, Wu X, et al. Method for perfusion decellularization of porcine whole liver and kidney for use as a scaffold for clinical-scale bioengineering engrafts. Xenotransplantation. 2015; 22(1): 48-61.
24. Wang LR, Lin YQ, Wang JT, Pan LL, Huang KT, Wan L, et al. Recent advances in re-engineered liver: de-cellularization and re-cellularization techniques. Cytotherapy. 2015; 17(8): 1015-1024.
25. Soto-Gutierrez A, Zhang L, Medberry C, Fukumitsu K, Faulk D, Jiang H, et al. A whole-organ regenerative medicine approach for liver replacement. Tissue Eng Part C Methods. 2011; 17(6): 677-686.
26. Mazza G, Al-Akkad W, Telese A, Longato L, Urbani L, Robinson B, et al. Rapid production of human liver scaffolds for functional tissue engineering by high shear stress oscillation-decellularization. Sci Rep. 2017; 7(1): 5534.
27. Sabetkish S, Kajbafzadeh AM, Sabetkish N, Khorramirouz R, Akbarzadeh A, Seyedian SL, et al. Whole-organ tissue engineering: decellularization and recellularization of three-dimensional matrix liver scaffolds. J Biomed Mater Res A. 2015; 103(4): 1498-1508.
28. Eipel C, Abshagen K, Vollmar B. Regulation of hepatic blood flow: the hepatic arterial buffer response revisited. World J Gastroenterol. 2010; 16(48): 6046-6057.
29. Lautt WW. Hepatic circulation: physiology and pathophysiology. San Rafael (CA): Morgan & Claypool Life Sciences; 2009.
30. Treyer A, Musch A. Hepatocyte polarity. Compr Physiol. 2013; 3(1): 243-287.
31. Taylor DA, Kren SM, Rhett K, Robertson MJ, Morrissey J, Rodriguez OE, et al. Characterization of perfusion decellularized whole animal body, isolated organs, and multi-organ systems for tissue engineering applications. Physiol Rep. 2021; 9(12): e14817.
32. Wu Q, Bao J, Zhou YJ, Wang YJ, Du ZG, Shi YJ, et al. Optimizing perfusion-decellularization methods of porcine livers for clinical-scale whole-organ bioengineering. Biomed Res Int. 2015; 2015: 785474.
33. Maghsoudlou P, Georgiades F, Smith H, Milan A, Shangaris P, Urbani L, et al. Optimization of liver decellularization maintains extracellular matrix micro-architecture and composition predisposing to effective cell seeding. PLoS One. 2016; 11(5): e0155324.
34. Willemse J, Verstegen MMA, Vermeulen A, Schurink IJ, Roest HP, van der Laan LJW, et al. Fast, robust and effective decellularization of whole human livers using mild detergents and pressure controlled perfusion. Mater Sci Eng C Mater Biol Appl. 2020; 108: 110200.
35. Gratzer PF, Harrison RD, Woods T. Matrix alteration and not residual sodium dodecyl sulfate cytotoxicity affects the cellular repopulation of a decellularized matrix. Tissue Eng. 2006; 12(10): 2975-2983.
36. Yang W, Xia R, Zhang Y, Zhang H, Bai L. Decellularized liver scaffold for liver regeneration. Methods Mol Biol. 2018; 1577: 11-23.
37. Hosseini V, Maroufi NF, Saghati S, Asadi N, Darabi M, Ahmad SNS, et al. Current progress in hepatic tissue regeneration by tissue engineering. J Transl Med. 2019; 17(1): 383.
38. Arzumanian VA, Kiseleva OI, Poverennaya EV. The curious case of the HepG2 cell line: 40 years of expertise. Int J Mol Sci. 2021; 22(23): 13135.
39. Cao Y, Gong Y, Liu L, Zhou Y, Fang X, Zhang C, et al. The use of human umbilical vein endothelial cells (HUVECs) as an in vitro model to assess the toxicity of nanoparticles to endothelium: a review. J Appl Toxicol. 2017; 37(12): 1359-1369.
40. Panwar A, Das P, Tan LP. 3D hepatic organoid-based advancements in liver tissue engineering. Bioengineering (Basel). 2021; 8(11): 185.